PLOS ONE

RESEARCH ARTICLE

An apta-aggregation based machine learning assay for rapid quantification of lysozyme through texture parameters

Manoharan Sanjay[1], Kumar Gaurav[2], Maria Jesus Gonzalez-Pabon[1], Julio Fuchs[1], Susan R. Mikkelsen[3], Eduardo Cortón[1] *

1 Biosensors and Bioanalysis Laboratory (LABB), Department of Biological Chemistry and IQUIBICEN-CONICET, Exact and Natural Sciences Faculty (FCEN), University of Buenos Aires (UBA), Buenos Aires, Argentina, **2** Department of Biosciences and Bioengineering, Indian Institute of Technology Guwahati, Guwahati, Assam, India, **3** Department of Chemistry, University of Waterloo, Waterloo, Ontario, Canada

* eduardo@qb.fcen.uba.ar

Abstract

A novel assay technique that involves quantification of lysozyme (Lys) through machine learning is put forward here. This article reports the tendency of the well- documented Ellington group anti-Lys aptamer, to produce aggregates when exposed to Lys. This property of apta-aggregation has been exploited here to develop an assay that quantifies the Lys using texture and area parameters from a photograph of the elliptical aggregate mass through machine learning. Two assay sets were made for the experimental procedure: one with high Lys concentration between 25–100 mM and another with low concentration between 1–20 mM. The high concentration set had a sample volume of 10 μl while the low concentration set had a higher sample volume of 100 μl, in order to obtain the statistical texture values reliably from the aggregate mass. The platform exhibited an experimental limit of detection of 1 mM and a response time of less than 10 seconds. Further, two potential operating modes for the aptamer were hypothesized for this aggregation property and the more accurate mode among the two was ascertained through bioinformatics studies.

Introduction

Agglutination is a term that is generally confined to antibody-antigen interactions that result in an interlinked mass of antigens and antibodies. It is commonly used in ABO blood typing where antibodies attached to latex particles are mixed with the blood sample. When these antibodies crosslink with a polyvalent antigen it results in agglutination or precipitation of particles [1, 2]. Besides blood-typing, agglutination techniques were also historically used for classifying beta-hemolytic streptococci based on antigenic differences through anti-sera [3]. This is an example of a direct/active agglutination assay, since the Streptococci have an inherent tendency to agglutinate. When the aggregate visualization is enhanced by the attachment to inert latex beads it qualifies as passive agglutination assay as the agglutination of the beads indicates the presence of an antibody binding to some other antigen [4]. Agglutination assays

are inexpensive, since agglutination can be detected visually. Additionally they are simple, rapid, often requiring only a few minutes and offer a high degree of sensitivity [5]. A plethora of assays based on antibodies have been explored. A few such assays include the latex beads-facilitated antibody agglutination assay for *Tritrichomonas foetus* described by Schaut *et al.*, [6], measurement of von Willebrand factor antigen through a latex agglutination test illustrated by Mahat *et al.* [7], and a microfluidic immuno-magnetic agglutination assay for detection of dengue virus NS1 antigen published by Alejo-Cancho *et al.*, [8].

However, the main disadvantage of this technique along with its qualitative/semi-quantitative nature is its use of antibodies [9]. The involvement of antibodies renders these assays temperature-sensitive and drives up the cost per test due to the high costs involved in antibody production and purification [10, 11]. In that context, new-generation of affinity molecules like aptamers are being widely preferred due to their effectiveness and robustness [12]. Aptamers have already found application in several bioassay modalities such as Quartz crystal microbalance [13, 14], Cantilever-based biosensing [15, 16], electrochemistry [17], Surface plasmon resonance [18, 19] and spectrophotometric assays [20].

The usage of aptamers in aggregation assays is not widely explored because of the monovalency of the aptamer towards the analyte. Agglutination assays strictly require both the analyte and the ligand to be polyvalent. Unlike the bivalent IgA antibody or the polyvalent IgM antibody, aptamers possess only a single binding site. Further, the analyte in question, at most instances possesses only a single binding site. This is generally circumvented by coupling aptamers to microbeads as it imparts polyvalency to the beads and facilitates agglutination. Polystyrene micro/nano beads were utilized to illustrate the same by Kim *et al.*, and the agglutination mass was quantified through a simple light scattering assay [21]. In the study by Uddin *et al.*, aptamer coated magnetic beads were used for agglutination to facilitate an optomagnetic readout [22]. The problem of antigen polyvalency is often overlooked by opting for inherently polyvalent analytes. Cells are often the best candidates as their exteriors are covered with numerous antigens of the same kind thereby rendering them polyvalent. For instance, the numerous lipophosphoglycan molecules that coat the surface of *Tritrichomonas foetus* have been capitalized for the development of an agglutination assay [6]. Hence, agglutination assays for other kinds of analytes without polyvalent beads remains to be researched.

Turbidimetry and optomagnetism-based detection are the widely used techniques for quantification of agglutination assays. Turbidimetry involves the process of measuring the loss of transmitted light intensity due to the scattering effect of particles suspended in it and it is determined through a microtiter-plate reader [23]. The optomagnetic detection technique employs a Blu-ray optical pickup unit as the excitation element, a photodetector as the sensing element and an AC magnetic field to provide the excitation energy. When the magnetic beads agglutinate, they exhibit optical anisotropy upon application of the oscillating magnetic field. Due to the large size of these agglomerates, the dynamics of this process is shifted to frequencies well below the Brownian relaxation frequency of the individual beads and this is interrogated through a photodetector [24]. These large, expensive and complex quantification equipment confine aggregation assays to lab-scale measurements despite the simplicity of these reactions. In that context, there is a need for inexpensive quantification platforms and smartphones with their state-of-the-art components and computation power coupled with their easy availability make for ideal candidates. Hence, we present here a novel apta-aggregation assay, where Lys containing samples are placed as droplets on a substrate followed by dropping the anti-Lys aptamer solution. Lys was quantified by employing a neural network trained with texture parameters and area of the aggregate mass obtained through a photograph taken with a smartphone and without the use of polyvalent microbeads as shown in Fig 1. The
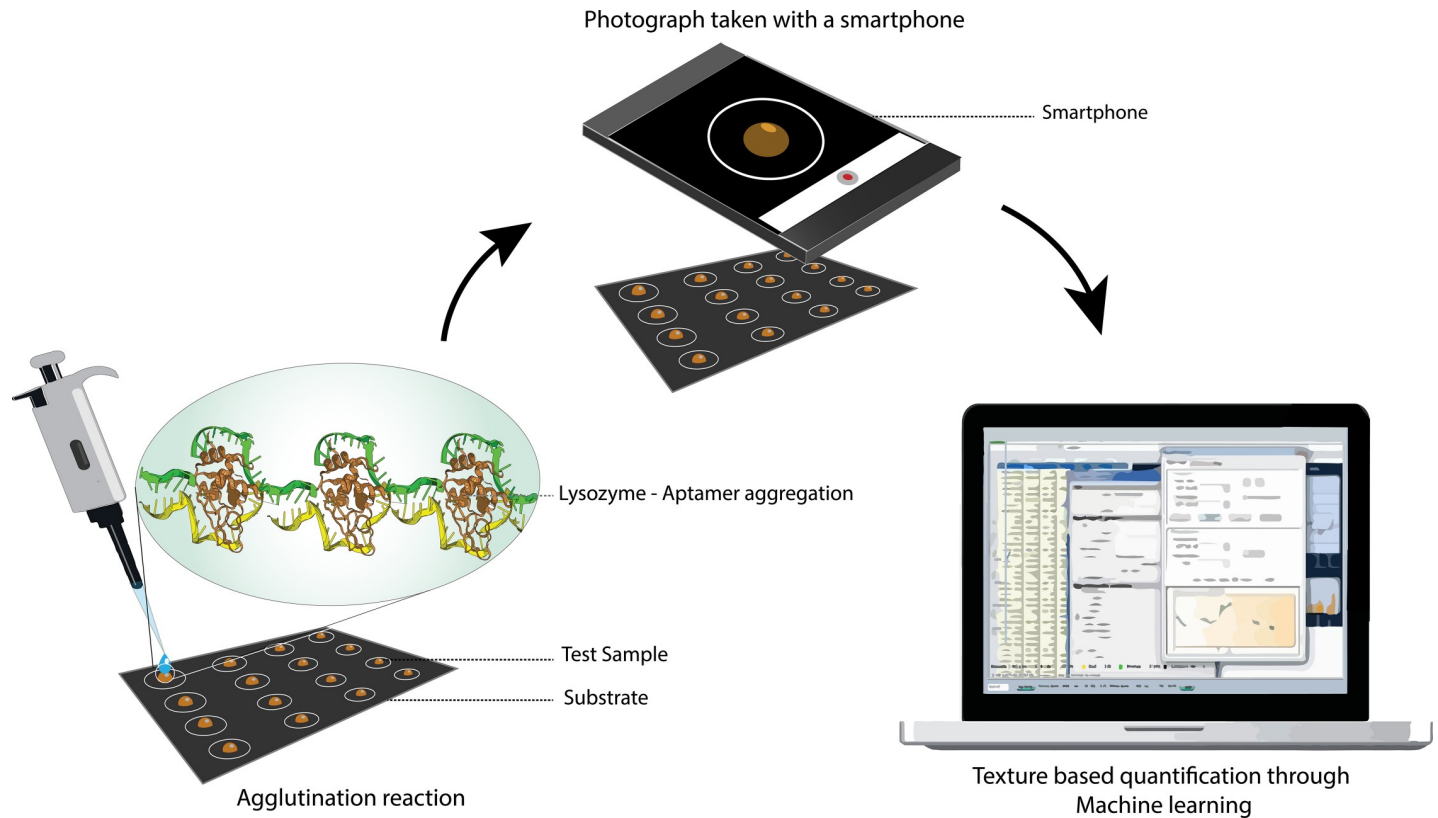
Fig 1. Steps involved in the quantification of the apta-aggregation assay.

Ellington *et al.*, anti-lys aptamer has been used for the purpose and its efficiency and specificity has been verified extensively through different transduction mechanisms in literature [25–30].

A direct way to quantify aggregation could be through histogram analysis of captured photos but its reproducibility issues have raised major concerns in the past [31]. Alternatively, establishing a relationship between aggregate area and Lys concentration for quantification could be a straight-forward approach as well. However, this is more complicated than it sounds, as the area can be greatly affected by the way in which the aptamer solution is dropped over the Lys droplet such as the trajectory, height from which it is dropped and angle of the drop. Whilst controlling these parameters is impossible without automation, a more logical way forward is to exploit the aggregate area-texture relationship. For a constant concentration of aptamer and lysozyme, the texture of its aggregate mass changes with the aggregate area due to variabilities in the aptamer dropping i.e., an aggregate mass of a small area will be coarse and compact while a large area aggregate will be smooth and diffused. Hence, this interplay of texture and aggregate area has been capitalized for this assay. The use of free aptamers in solution to detect a wide range of protein analytes ranging from C-Reactive Protein to Plasmodium Lactate dehydrogenase has been reported widely in literature via gold nanoparticle (GNP) aggregation assays [32–34]. Lysozyme has also been previously quantified using an assay with gold nanoparticles and anti-lys 25 base pair aptamer by Yao *et al.*, [35]. The use of GNPs adds to the cost and complexity, all the while suffering from the previously mentioned shortcomings of histogram-based quantification. However, the prior existence of these assays including the one with lysozyme by Yao *et al.*, verified the feasibility and laid the foundation for the texture-based quantitative assay devoid of Gold-nanoparticles and polyvalent beads.

The texture of an image can be defined as the spatial grouping of color or intensities in an image or selected region of an image. A statistical method for studying texture is through gray-level co-occurrence matrix (GLCM), which considers the spatial relationship of pixels. The GLCM functions characterize the texture of an image by determining the frequency of occurrence of pairs of pixels with specific values and in a specified spatial relationship in an image to create a GLCM. The statistical functions are extracted from this matrix which act as indicators of the image texture [36, 37]. Texture parameters extraction is often coupled with machine learning and has been widely used in remote sensing [38] and even for cancer classification or diagnosis from computer tomography, ultrasound and MRI images [39–41].

Aggregation without polyvalent microbeads was made possible through the unique aggregation property demonstrated by the anti-Lys aptamer uncovered by this study. The requirement of polyvalency of both aptamer and protein for aggregation assays has been highlighted previously [20]. In that light, the ability of this aptamer to form aggregates on exposure to Lys made us hypothesize two modes-of-interaction Mode.1- Lys has two binding sites for the aptamer and the aptamer has two binding sites for Lys or Mode.2- Lys has two binding sites for aptamer but aptamer does not contain two binding sites for Lys, instead it binds to adjacent Lys-bound aptamers through Watson-Crick complementary base pairing. In order to unravel the mode of operation, bioinformatics tools such as RNA composer and HDock were employed. This part of the study provided insights into the inner workings of all aptamer-analyte interactions in general and can potentially prove useful for future aptamer design and development.

Materials and methods

Aggregation reaction

Lysozyme from hen's egg white dissolved in ultrapure water (= 18.2 MΩ) from a Millipore-MilliQ system at different concentrations was used as the test sample. Lysozyme from chicken egg white and bovine serum albumin (BSA), were purchased from Sigma–Aldrich. The DNA-anti-Lys aptamer developed by Ellington *et al*., (5′-ATC TAC GAA TTC ATC AGG GCTAAA GAG TGC AGA GTT ACT TAG-3') was purchased from Integrated DNA Technologies, Inc. [42]. The anti-Lys aptamer was heated at 70˚C for 3 minutes before exposure to Lys. This is essential for preserving the structural capabilities and increasing the efficiency of analyte capture [26]. Two sets of Lys test samples were prepared, a high concentration set "A" (25 mM-400mM) and a low concentration set "B" (1–20 mM). The Set-A assay sample volume was fixed to 10 μl and the B set volume to 100 μl. Lower concentrations (set "B") produced no visible aggregates or micro aggregates that were not resolvable by the smartphone camera when using 10 μl sample volume. Hence by choosing a higher sample volume among lower analyte concentrations, more lysozyme molecules were available for aggregation and therefore a visually resolvable aggregate mass, increasing the concentration range that can be measured. These samples were placed on a reaction substrate using a micropipette and studied as triplicates. The reaction substrate was made by printing an image containing 35 circular reaction areas on a black background on a generic photographic paper as seen in Fig 1. The hydrophobicity of the photo paper was evaluated as per Chen *et al*., [43]. The liquid-substrate contact angle was found to be 94.686˚ indicating that it is hydrophobic [44]. This hydrophobic property along with the surface tension of droplets provided resulted in reaction droplets of fairly similar geometry. The test samples were then exposed to heat treated 3 μl aptamer solution of 25 nM concentration followed by waiting for approximately a minute after which the aggregates were observed. The 3 μl aptamer solution volume was finalized following an experiment to determine the effect of aptamer volume on aggregation intensity. In short, five 10 μl Lys reaction

droplets of 25 mM concentration each were exposed to aptamer volumes between 1 μl to 5 μl and made up to 15 μl followed by studying their individual aggregation intensities. All the reactions were carried out directly on a lab bench at 20˚C and a relative humidity of 70–90%. The results from the triplicates, formed the training data for the neural network. The test samples to evaluate the neural network were made along with the training triplicates with set concentrations of Lys. Further, the occurrence of aggregation exclusively to the Anti-lys aptamer-Lysozyme (Apta-Lys) samples was confirmed with a control (10 μl of 25 mM lysozyme alone), Negative control (25 mM BSA+ Anti-Lys aptamer) and the test condition (3 μl of anti-lys aptamer with 10 μl of 100 mM lysozyme).

Texture analysis and machine learning

The aggregates were then photographed using Oppo CPH1919 smartphone with a 48 Megapixel pixel-binning CMOS sensor (Sony IMX586) and analyzed using Image-J in a computer. These images were first converted into 8-bit and then their aggregate areas (Area) were measured via free-hand selection. Secondly, their texture was analyzed using GLCM texture plug-in V 0.4 developed by Julio E. Cabrera [45]. Various statistical parameters of the GLCM of the image such as Angular Second Moment (ASM), Inverse Difference moment (IDM), Entropy, Contrast and Correlation were provided by the plug-in. Triplicates were made and their statistical texture values along with the area of the aggregates were loaded as the training data for the neural network with a 6–1 architecture. Neural networking was performed by NeuroXL Predictor, a neural network-based add-in for Microsoft Excel developed by OLSOFT and is capable of advanced data forecasting, classification and clustering [46, 47]. The trained neural network was then tested with the data from a new set of Lys samples of pre-determined concentrations.

Bioinformatics analyses

The mode of the aptamer can be deduced through docking studies for which the 3-D structure of the aptamer has to be first predicted. Currently, there are no tools for direct DNA 3-D structure prediction while direct tools for RNA structure prediction exist. This problem has been previously circumvented through an ingenious ssRNA-ssDNA conversion strategy as illustrated by Jeddi *et al.*, and Alshaer *et al.*, [48, 49].

A similar strategy as it was previously detailed described [48, 49] to model the 3-D structure of the aptamers has been implemented here and it involves the following steps- i) generation of ssDNA secondary structure through RNAfold webserver [50] ii) construction of equivalent 3D ssRNA models using RNA Composer [51] iii) translation of 3D ssRNA models into ssDNA models through manual modification of the hydroxyl (OH) group at the 2'- Carbon of the ribose with a hydrogen atom and replacing all thymine molecules with uracil. and iv) finally refining the 3D ssDNA structures through energy minimization using a CHARMM force field and 10000 steps of gradient energy minimization method using NAMD software [52, 53]. The docking simulation was performed between the predicted aptamer and the X-ray structure of the Lysozyme obtained from RCSB PDB database (PDB ID: 1DPX, Resolution: 1.65 Å) using HDOCK online server and the best pose was considered for all further studies [54]. In brief, one minimized aptamer was docked with lysozyme to get Lys-Apt models. The top 10 Lys-Apt models were re-docked with another aptamer to get Apt-Lys-Apt models. The top 10 models of each Apt-Lys-Apt model were analysed (100 models in toto). The model with the highest dock score without congruent binding sites was considered for further studies.

Further, in the event of Mode 2 (one bound aptamer hybridizing with neighbouring aptamer) being true, a strategy was devised to probe its probability by estimating the dock score of

the hairpin formed by the free terminals of the Lys-bound aptamer using VFold2D and the ΔG value of the neighbour strand hybridization, if any using VFoldCPX server [55]. These servers do not provide DNA interaction data and hence the output from these servers were to be converted later to DNA manually in PyMOL [56].

Finally, the 3-D structure of the polymeric complex was to be visualized through the following steps—i) Acquiring the secondary structure of neighbour aptamer interaction using VfoldCPX. Since the input of two single strands is not allowed and the energetics of RNA-RNA interaction are similar to intra-molecular RNA folding, the potential hybridized strands were concatenated with non-sequential residues (AAA) and the same RNA folding algorithm as in Vfold2D server was to be utilized ii) Obtaining its tertiary structure by inputting Vfold2D output to RNAcomposer iii) Deletion of the non-sequential residues from both the 3D and 2D outputs iv) Manual conversion of all the outputs to DNA [55, 57–61]. It was to be followed by manually coupling two Aptamer-Protein-Aptamer complexes with the obtained hybridized aptamer ends to construct the probable structure of the polymeric complex. Finally, any non-specific interactions between the two aptamers bound to the lysozyme was probed by manually deleting the lysozyme from the complex and detecting the potential interactions using PPCheck webserver [62].

Results and discussion

Aggregation assay

The occurrence of aggregation exclusively to Apta-Lys samples was confirmed by comparing the texture from a control, negative control and test condition as shown in Fig 2B. There was no observable texture change in the controls whereas the test condition revealed an aggregate mass. Then the effect of aptamer concentration on aggregation intensity was examined. The aggregation area was found to have an almost linear relationship with the aptamer quantity and visually the aggregation intensity was also higher with high volume, with the 5 μl droplet volume showing the highest aggregation area. However, the 3 μl droplet was experimentally shown to produce a high volume to aggregate area ratio thereby making it an efficient option as illustrated by Fig 2A; at S4 Fig in S1 File the characteristic and LOD in order to determine the minimal amount of aptamer needed to perform one analysis in this condition is also shown. Therefore, the 3 μl aptamer volume was chosen for all further experiments.

Additional experiments were conducted to evaluate the dose response and it was found that lower concentrations of Lys produced barely observable aggregation. Hence the sample volume was increased to 100 μl, which in turn increased the number of Lys molecules available for the reaction. This formed the rationale behind the two sets of experiments namely, Set-A and Set-B. Both Set-A and Set-B, exhibited higher aggregation intensity with increasing concentrations. However, the area of aggregation varied widely. The Set-A displayed dense, increasingly intense, larger area aggregates in higher concentration samples because there are progressively more Lys molecules for the same volume to aggregate. In contrast, Set-B produced diffuse, less intense, larger area aggregates for low concentration and dense, small-area aggregates for high concentrations as portrayed by Fig 4. This can be attributed to the higher sample volume of Set-B. At 100 μl volume, low concentration samples are sparsely populated with Lys molecules which may mean that the aptamers, when dropped over the samples have to travel further in order to find their Lys molecules and aggregate. This may lead to thin or disjointed chains of Apta-Lys that precipitate thereby producing hazy, large area aggregates.

On the other hand, a high concentration sample is densely populated with Lys and hence the aptamers have to travel less to find their Lys molecules which means that highly dense Apta-Lys chains are formed quickly and precipitate without much dispersion. This potential
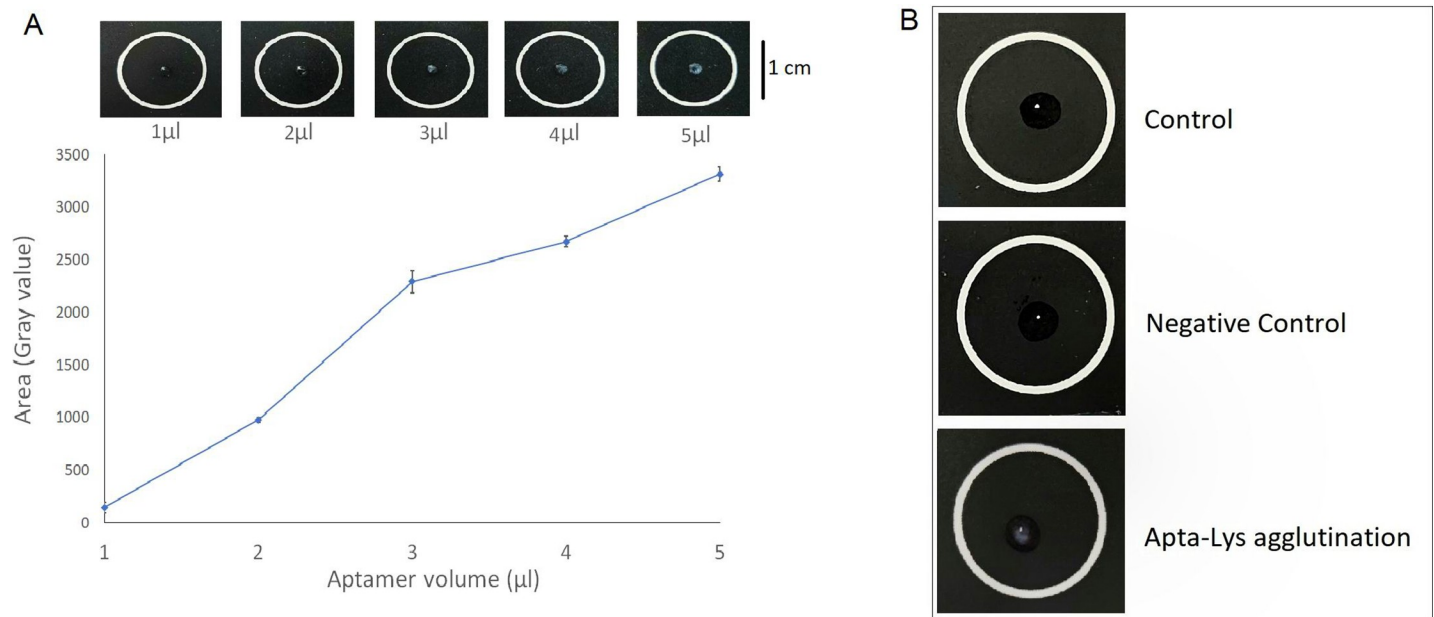
Fig 2. Aggregation assay. A) Impact of aptamer volume on aggregate area B) Test to confirm the exclusivity of aggregation to Anti-Lys aptamer and lysozyme.

explanation for the phenomenon is illustrated in Fig 3. In brief, the lower concentrations-higher sample volume of Set-B and higher concentrations-smaller sample volume of Set-A led to a clear distinction in the aggregation dynamics. Though the area varied, increasingly intense masses were observed with high concentrations among both the sets and these masses seemed to exhibit a similar textural statistics trend as seen in Fig 4; some analysis about the sensitivity of each parameter shown is presented in S1 and S2 Tables in S1 File.

The angular second moment (ASM) is a measure of homogeneity of the texels while contrast is a measure of the amount of local variations existing in an image. Correlation represents how a reference pixel is related to its neighbour pixel, and can have values between -1 (perfectly correlated) to 1 with a value of 0 representing no correlation and masses with considerable amounts of linear structures can project high correlation. Inverse difference moment
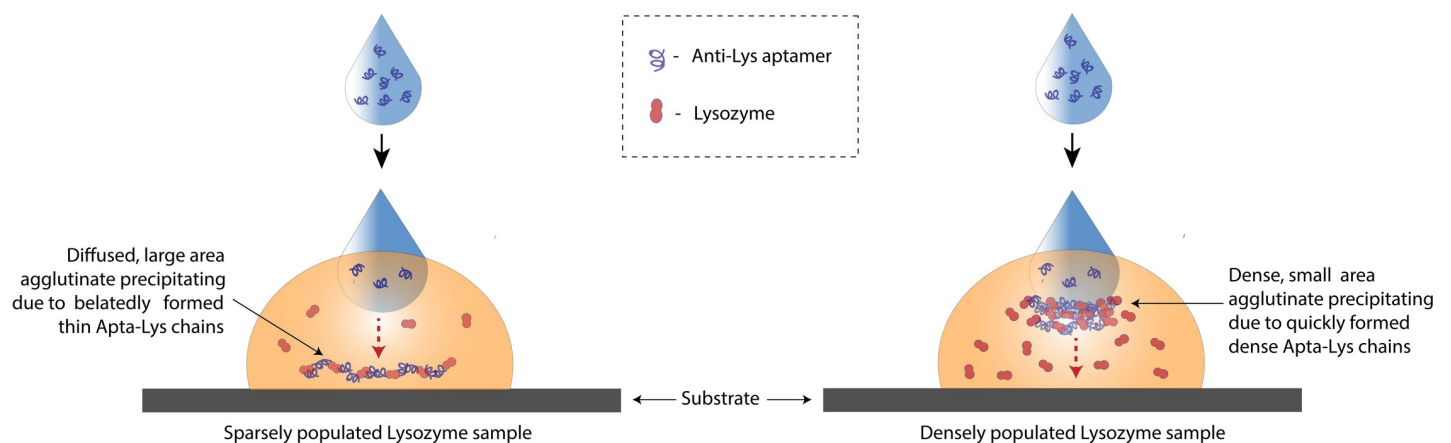

Fig 3. Formation of aggregates. Left, in sparsely populated (low concentration) and right, densely populated (high concentration) lysozyme samples.
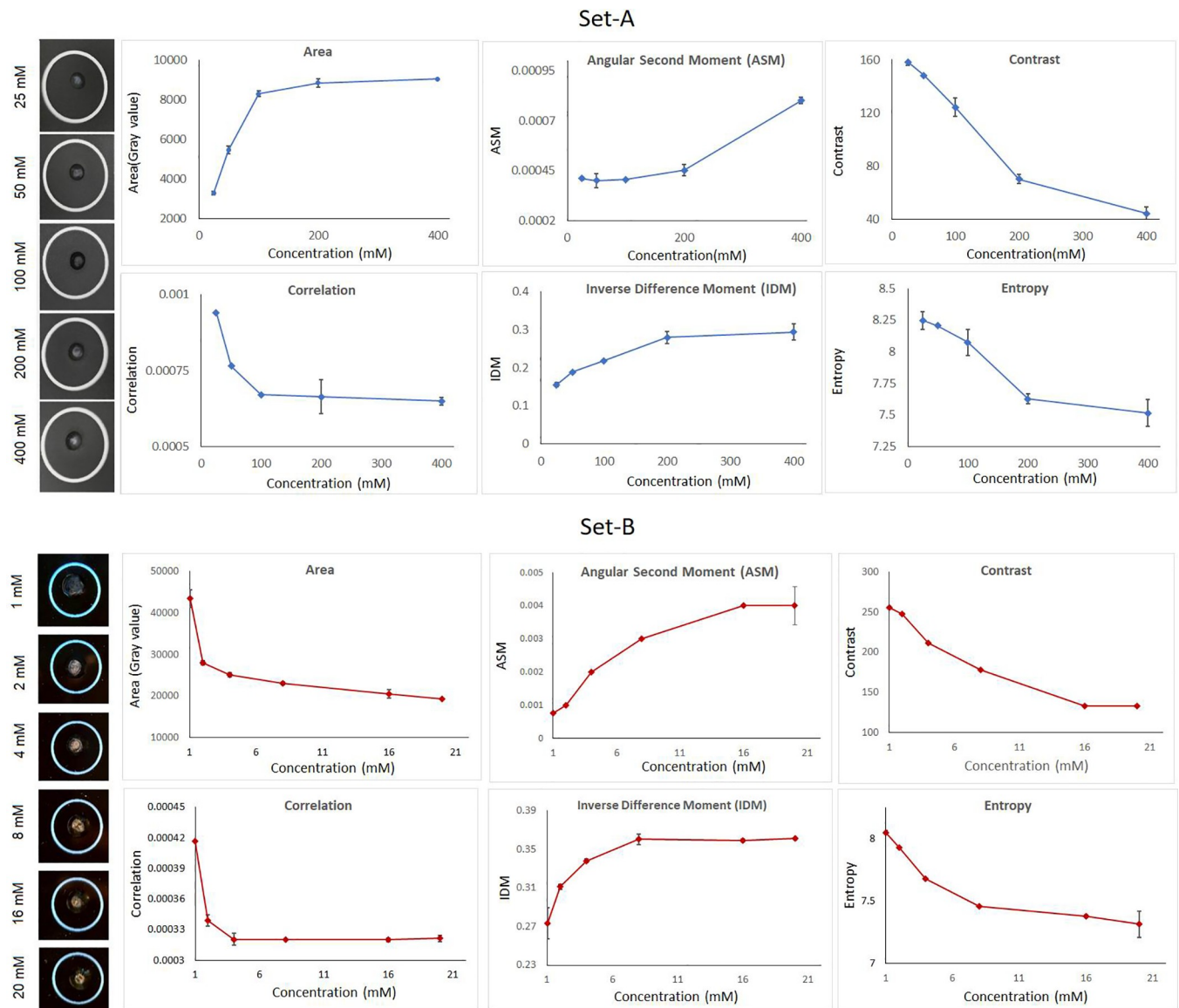
Fig 4. Texture parameters extracted from the aggregate masses.

(IDM) is the measure of local homogeneity and increases with the quantity of linear structures in an image. High entropy usually implies elevated level of disorder and disorganization [36, 63–65]. In brief, ASM and IDM are indicators of homogeneity while contrast, correlation and entropy are indicators of chaos in the image. The trends of these parameters of both the sets indicated that increasingly homogenous and less chaotic masses are produced with higher concentrations as depicted by Fig 4. and two separate training models for Set- A and for Set-B were used for the neural network. The trained neural networks were used to predict the concentrations of the test set through the texture parameters extracted from a predetermined set of concentrations as mentioned in the previous section. The learning process of the model and the deviation between the predicted values and expected values of the test set are shown in Fig 5. On the whole, the efficiency of the prediction process was found to be approximately 96.365%, indicating that there is a slight deviation between the predictions and the actual
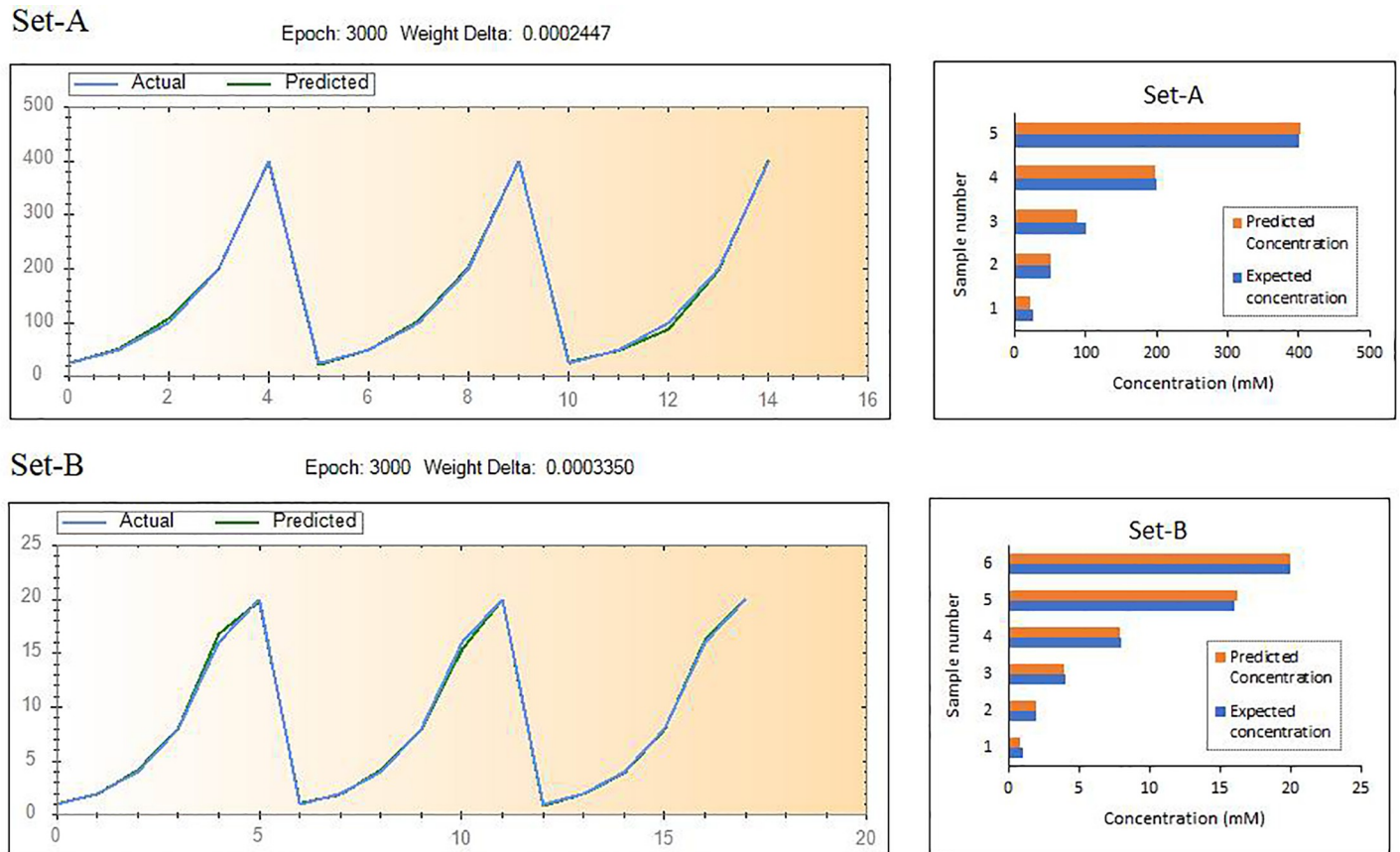
Fig 5. Trained model and the deviation of the predicted results from the expected values.

values ([Fig 5](#)). This can possibly be rectified by increasing the training sample size as generally, it is inferred that using sufficient data set for predictive model construction can lead to better accuracy [66].

DNA structure prediction and docking

The predicted 3-D structure of the aptamer obtained from RNA Composer (S1 Fig in S1 File) and minimized using NAMD (S2 Fig in S1 File) suggested that the 5'-ter of the aptamer wrapped the protein while the 3'-ter produced a hairpin loop that made no contact with Lys ([Fig 6](#)), indicating the absence of any role for 3'-ter in the Lys binding. In order to identify the appropriate mode among the two hypothesized for the aptamer, the aptamer was docked with lysozyme and the top 10 Lys-Apt models were re-docked with another aptamer molecule to get another set of top 10 model Apt-Lys-Apt models. Among the 100 resultant models, the one without congruent sites with the highest dock score was considered. The successful model possessed a dock score of -267.68 and an RMSD of 62.64 while the second binding site exhibited a dock score of -369.82 and an RMSD of 45.50. The bonds involved in both the binding sites were uncovered, as shown in [Fig 6](#). The aptamer produced very few interactions with the protein side chain which is expected as the aptamer screening SELEX process is performed with the protein in its native structure and presents very few side-chains facing the exterior of the protein.
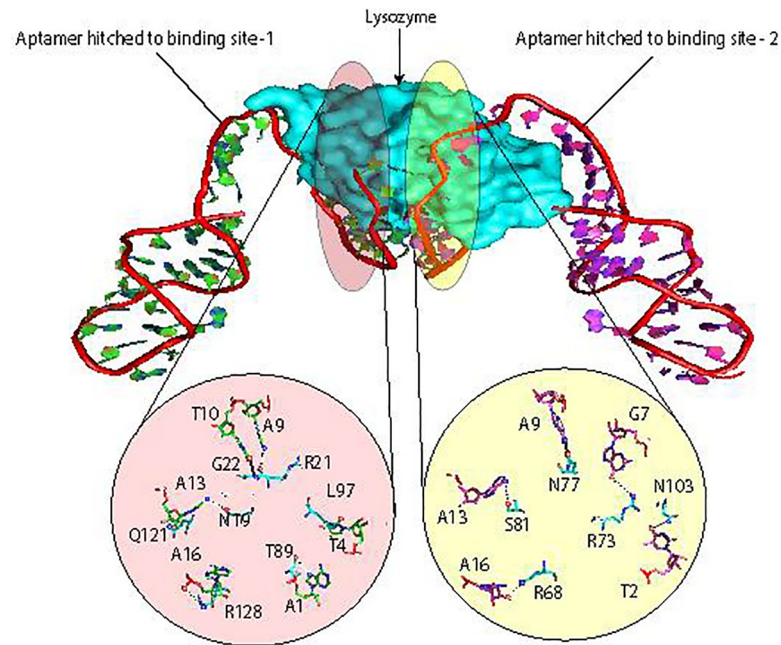
Fig 6. Lysozyme with two anti-Lys aptamers bound to its two binding sites.

The aptamers bound to both the sites had free 3'-terminals which indicated the lack of any role for 3'-ter in the protein interaction. This suggested that mode 1 is not probable and mode 2 is more prospective. In order to probe the same (neighbour-aptamer interaction), the free 3'-terminal of the aptamer which formed a hairpin was severed. This severed terminal was then subjected to hairpin binding energy and heterodimer formation analysis as a higher binding energy for the heterodimer (neighbour aptamer interaction) would indicate its spontaneity over hairpin formation. Subsequently, the binding energy of the 3'-ter hairpin (-3.81 Kcal/mol) calculated using Vfold2D web server (S3 Fig in S1 File) was found to be lesser than the binding energy (-11.70 Kcal/mol) of the 3'-ter double strand (neighbour-aptamer interaction) calculated using VfoldCPX web server.

This exercise exemplified Mode-2 as the probable cause for formation of aggregates with one Apta-Lys-Apta complex acting as a monomeric unit. The potential 3-D structure of this polymeric complex was then constructed by merging the 3-D structure output of 3'-ter inter-actions obtained from RNAcomposer with the previously obtained Apta-Lys-Apta complex as shown in Fig 7. The accuracy of the docked poses hold more room for improvement since the rigid docking strategy followed here is less precise due to the lack of conformational flexibility of the lysozyme and aptamer [67]. It further disregards the solvent and entropic contributions to the binding free energy and hence these calculations are also required for further accuracy [68].

This work focuses on the detection of Lys, a significant biomarker for many diseases how-ever it is not specific to any particular ailment. Nevertheless, we believe that this research holds a lot of promise for custom designing future aptamers for physiologically more significant bio-markers. The significance of finding multiple binding sites on a protein for the same aptamer like the current study, is not just limited to aggregation assay development. It can also be extended to development of novel sandwich assays and innovative in-vivo aptamer-based treatment procedures. The LOD achieved by this method through normal photography
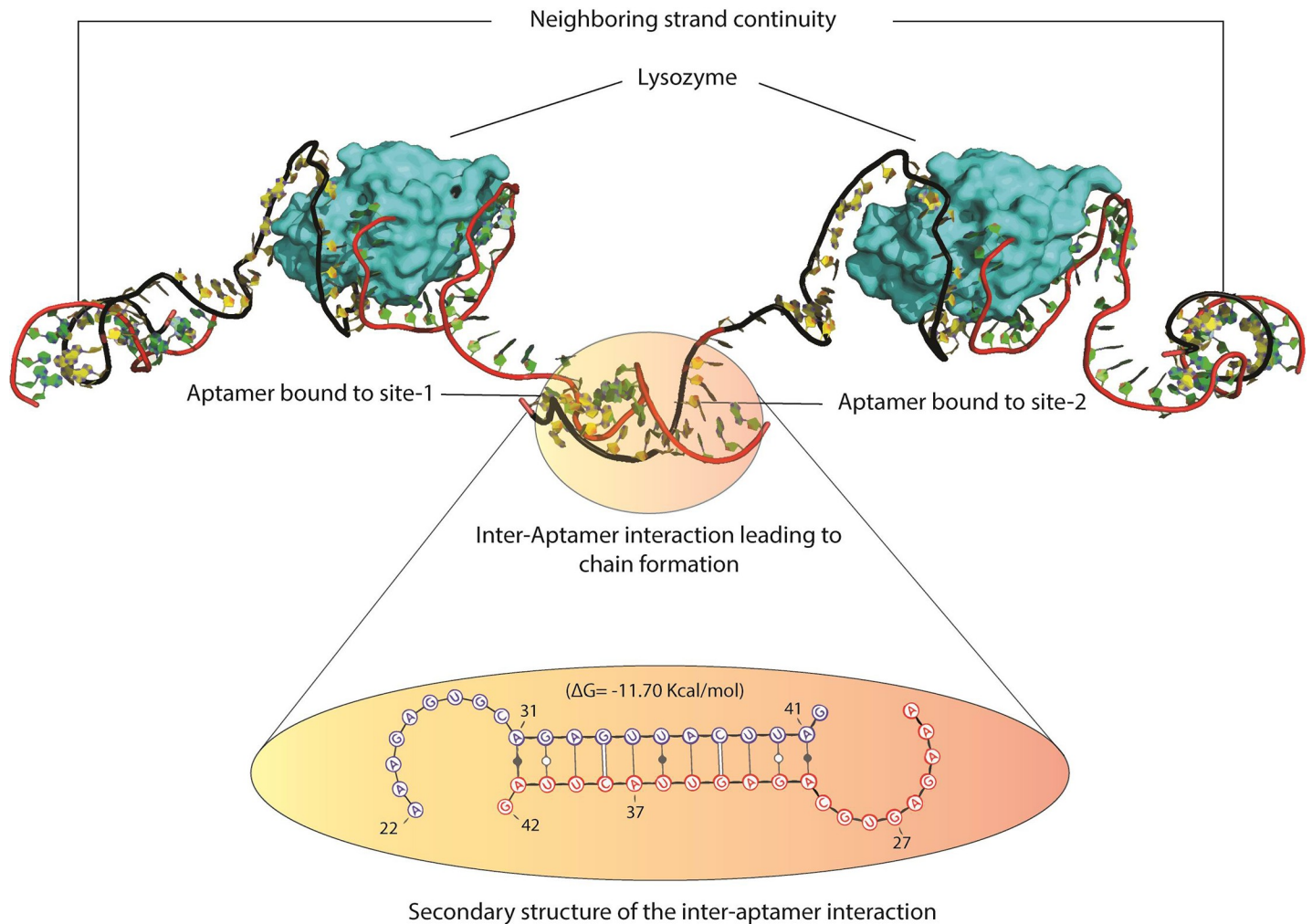
Neighboring strand continuity

Lysozyme

Aptamer bound to site-1

Aptamer bound to site-2

Inter-Aptamer interaction leading to
chain formation

(ΔG= -11.70 Kcal/mol)

31

41

37

22

42

27

Secondary structure of the inter-aptamer interaction

Fig 7. Representation of the polymeric chain highlighting the interacting base pairs in the inter-aptamer interaction.

prevails in the mM range because of the invisibility of micro-aggregates to the naked eye. A better LOD can be achieved through texture analysis of photographs of microscopic images or with sensitive turbidimetric instruments. In that perspective, point-of-care capabilities with low LODs can be realized in subsequent investigations through the development of compact optical setups for photomicrography or ultra-portable turbidimetric equipment. Additionally, the results obtained from the neural network exhibited a slight deviation from the expected values. This can be rectified with a higher sample size. However, the vagueness that surrounds the impact of the dataset size on prediction accuracy makes it difficult to say precisely when a dataset is big enough to provide accurate results, which makes this another future direction for study [44]. Finally, upcoming studies can be geared towards solidifying the underlying principle and augment the current bioinformatics studies with crystallographic data. We believe that these are the key areas that can steer future research in this highly promising direction.

Conclusions

Herein, we have described a novel assay technique to quantify Lys via texture analysis and neural networking. Further, we probed into the molecular workings of the aptamer-analyte

interaction responsible for the aggregation property, through bioinformatics tools. The significance of this study lies on two fronts- the bioinformatics analysis and the assay technique. The bioinformatics part of the article sheds light to the mode of aptamer-analyte interaction, a mechanism that can be useful for rational re-design/improvement of screened aptamers. This workflow presents many untapped aptamer-analyte properties that could be exploited for novel assay development. On that pretext, this article explores the aggregation property of the Ellington-group aptamer and exploits it for quantification using a beadless aptamer aggregation assay. On the assay front, the texture-based quantification reported here further expands the ever-growing repertoire of novel quantification techniques. Quantification of aggregation is generally facilitated by complex laboratory equipment thereby making them unfit for point-of-care and low-cost applications. Nonetheless, this article circumvents the problem by using a smartphone and a computer leading to low assay cost and higher point-of-care capability. The limit of detection of this method was experimentally found to be 1 mM and the volume of sample used for detection was 10 μl for 25–400 mM range and 100 μl for 1–20 mM range.

Supporting information

S1 File.
(DOCX)

Acknowledgments

We want to acknowledge the support of IQUIBICEN technical and administrative personnel, as well to the International Cooperation Office at the Facultad de Ciencias Exactas y Naturales, which smooth the intricate paperwork necessary to allow one of us reaching Argentina from India (M.S.).

Author Contributions

Conceptualization: Manoharan Sanjay, Kumar Gaurav.

Data curation: Manoharan Sanjay.

Formal analysis: Manoharan Sanjay.

Funding acquisition: Julio Fuchs, Eduardo Cortón.

Investigation: Manoharan Sanjay, Kumar Gaurav, Maria Jesus Gonzalez-Pabon.

Methodology: Manoharan Sanjay, Kumar Gaurav, Maria Jesus Gonzalez-Pabon.

Project administration: Eduardo Cortón.

Resources: Julio Fuchs, Eduardo Cortón.

Software: Kumar Gaurav.

Supervision: Eduardo Cortón.

Validation: Susan R. Mikkelsen.

Writing – original draft: Manoharan Sanjay, Kumar Gaurav.

Writing – review & editing: Susan R. Mikkelsen, Eduardo Cortón.

References

1. Gibbons I (1989) US4829011A - Agglutination assay. U.S. Patent No. 4,829,011.

2.   Harmening DM (2019) Modern Blood Banking and Transfusion Practices. 7th Ed. FA Davis.

3.   Lancefield RC (1928) The antigenic complex of *Streptococcus ilemolyticus*: II. Chemical and immuno-logical properties of the protein fractions. J. Exp. Med. 47: 469–480. https://doi.org/10.1084/jem.47.3.469 PMID: 19869424

4.   Bray RS, Lainson R (1967) Studies on the immunology and serology of Leishmaniasis V. The use of particles as vehicles in passive agglutination tests. Trans. R. Soc. Trop. Med. Hyg. 61: 490–505. https://doi.org/10.1016/0035-9203(67)90099-5 PMID: 4964087

5.   Alhabbab RY (2018) Precipitation and Agglutination Reactions. Springer, Cham; pp. 23–30. https://doi.org/10.1007/978-3-319-77694-1_3

6.   Schaut RG, Corbeil LB, Blake CN, Brewer MT (2017) Development of a bead-agglutination assay for rapid detection of *Tritrichomonas foetus*. Vet. Parasitol. 243: 188–191. https://doi.org/10.1016/j.vetpar.2017.06.025 PMID: 28807292

7.   Mahat M, Abdullah WZ, Che Hussin CM (2014) Conventional rapid latex agglutination in estimation of von willebrand factor: Method revisited and potential clinical applications. J. Immunol. Res. 2014: 850810. https://doi.org/10.1155/2014/850810 PMID: 25759835

8.   Alejo-Cancho I, Navero-Castillejos J, Peiró-Mestres A, Albarracín R, Barrachina J, Navarro A, et al. (2020) Evaluation of a novel microfluidic immuno-magnetic agglutination assay method for detection of dengue virus NS1 antigen. Forshey BM, editor. PLoS Negl. Trop. Dis. 14: e0008082. https://doi.org/10.1371/journal.pntd.0008082 PMID: 32069280

9.   Stavitsky AB (1998) Agglutination. Encyclopedia of Immunology. Elsevier. pp. 56–59. https://doi.org/10.1006/rwei.1999.0016

10. Thiviyanathan V, Gorenstein DG (2012) Aptamers and the next generation of diagnostic reagents. Pro-teomics—Clinical Applications. NIH Public Access. pp. 563–573. https://doi.org/10.1002/prca.201200042 PMID: 23090891

11. Lakhin A V., Tarantul VZ, Gening LV (2013) Aptamers: Problems, solutions and prospects. Acta Natu-rae. Russian Federation Agency for Science and Innovation. pp. 34–43. https://doi.org/10.32607/20758251-2013-5-4-34-43 PMID: 24455181

12. Song KM, Lee S, Ban C (2012) Aptamers and their biological applications. Sensors 12: 612–631. https://doi.org/10.3390/s120100612 PMID: 22368488

13. Tombelli S, Minunni M, Luzi E, Mascini M (2005) Aptamer-based biosensors for the detection of HIV-1 Tat protein. Bioelectrochemistry 67: 135–141. https://doi.org/10.1016/j.bioelechem.2004.04.011 PMID: 16027048

14. Wang R, Li Y (2013) Hydrogel based QCM aptasensor for detection of avian influenza virus. Biosens. Bioelectron. 42: 148–155. https://doi.org/10.1016/j.bios.2012.10.038 PMID: 23202345

15. Chen X, Pan Y, Liu H, Bai X, Wang N, Zhang B (2016) Label-free detection of liver cancer cells by apta-mer-based microcantilever biosensor. Biosens Bioelectron. 79: 353–358. https://doi.org/10.1016/j.bios.2015.12.060 PMID: 26735868

16. Campbell GA, Mutharasan R (2007) A method of measuring *Escherichia coli* O157:H7 at 1 cell/mL in 1 liter sample using antibody functionalized piezoelectric-excited millimeter-sized cantilever sensor. Envi-ron. Sci. Technol. 41: 1668–1674. https://doi.org/10.1021/es061947p PMID: 17396658

17. Farid S, Meshik X, Choi M, Mukherjee S, Lan Y, Parikh D, et al. (2015) Detection of interferon gamma using graphene and aptamer based FET-like electrochemical biosensor. Biosens. Bioelectron. 71: 294–299. https://doi.org/10.1016/j.bios.2015.04.047 PMID: 25919809

18. Zhu Z, Feng M, Zuo L, Zhu Z, Wang F, Chen L, et al. (2015) An aptamer based surface plasmon reso-nance biosensor for the detection of ochratoxin A in wine and peanut oil. Biosens. Bioelectron. 65: 320–326. https://doi.org/10.1016/j.bios.2014.10.059 PMID: 25461176

19. Sanjay M, Singh NK, Ngashangva L, Goswami P (2020) A smartphone-based fiber-optic aptasensor for label-free detection of *Plasmodium falciparum* glutamate dehydrogenase. Anal. Methods. 12: 1333–1341. https://doi.org/10.1039/c9ay02406a

20. Zhou N, Zhang J, Tian Y (2014) Aptamer-based spectrophotometric detection of kanamycin in milk. Anal. Methods 6: 1569–1574. https://doi.org/10.1039/c3ay41816b

21. Kim K, Gu MB, Kang DH, Park JW, Song IH, Jung HS, et al. (2010) High-sensitivity detection of oxytet-racycline using light scattering agglutination assay with aptasensor. Electrophoresis 31: 3115–3120. https://doi.org/10.1002/elps.201000217 PMID: 20872613

22. Uddin R, Burger R, Donolato M, Fock J, Creagh M, Hansen MF, et al. (2016) Lab-on-a-disc agglutina-tion assay for protein detection by optomagnetic readout and optical imaging using nano- and micro-sized magnetic beads. Biosens. Bioelectron. 85: 351–357. https://doi.org/10.1016/j.bios.2016.05.023 PMID: 27183287

23. Petruševska M, Urleb U, Peternel L (2013) Evaluation of the light scattering and the turbidity microtiter plate-based methods for the detection of the excipient-mediated drug precipitation inhibition. Eur. J. Pharm. Biopharm. 85: 1148–1156. https://doi.org/10.1016/j.ejpb.2013.08.015 PMID: 24056092

24. Donolato M, Antunes P, de la Torre TZG, Hwu E Te, Chen CH, Burger R, et al. (2015) Quantification of rolling circle amplified DNA using magnetic nanobeads and a Blu-ray optical pick-up unit. Biosens. Bioelectron. 67: 649–655. https://doi.org/10.1016/j.bios.2014.09.097 PMID: 25453736

25. Rodriguez MC, Kawde AN, Wang J (2005) Aptamer biosensor for label-free impedance spectroscopy detection of proteins based on recognition-induced switching of the surface charge. Chem. Commun. 4267–4269. https://doi.org/10.1039/b506571b PMID: 16113717

26. Rodríguez MC, Rivas GA (2009) Label-free electrochemical aptasensor for the detection of lysozyme. Talanta 78: 212–216. https://doi.org/10.1016/j.talanta.2008.11.002 PMID: 19174227

27. Peng Y, Zhang D, Li Y, Qi H, Gao Q, Zhang C (2009) Label-free and sensitive faradic impedance aptasensor for the determination of lysozyme based on target-induced aptamer displacement. Biosens. Bioelectron. 25: 94–99. https://doi.org/10.1016/j.bios.2009.06.001 PMID: 19559590

28. Huang H, Jie G, Cui R, Zhu JJ (2009) DNA aptamer-based detection of lysozyme by an electrochemiluminescence assay coupled to quantum dots. Electrochem. Commun. 11: 816–818. https://doi.org/10.1016/j.elecom.2009.01.009

29. Cheng AKH, Ge B, Yu HZ (2007) Aptamer-based biosensors for label-free voltammetric detection of lysozyme. Anal. Chem. 79: 5158–5164. https://doi.org/10.1021/ac062214q PMID: 17566977

30. Kawde AN, Rodriguez MC, Lee TMH, Wang J (2005) Label-free bioelectronic detection of aptamer-protein interactions. Electrochem. Commun. 7: 537–540. https://doi.org/10.1016/j.elecom.2005.03.008

31. Kangas MJ, Burks RM, Atwater J, Lukowicz RM, Williams P, Holmes AE (2017) Colorimetric sensor arrays for the detection and identification of chemical weapons and explosives. Crit. Rev. Anal. Chem. 47: 138–153. https://doi.org/10.1080/10408347.2016.1233805 PMID: 27636675

32. António M, Ferreira R, Vitorino R, Daniel-da-Silva AL (2020) A simple aptamer-based colorimetric assay for rapid detection of C-reactive protein using gold nanoparticles. Talanta 214: 120868. https://doi.org/10.1016/j.talanta.2020.120868 PMID: 32278414

33. Jain P, Chakma B, Singh NK, Patra S, Goswami P (2016) Aromatic surfactant as aggregating agent for aptamer-gold nanoparticle-based detection of plasmodium lactate dehydrogenase. Mol. Biotechnol. 58: 497–508. https://doi.org/10.1007/s12033-016-9946-x PMID: 27189484

34. Sha H, Bin LD, Zhuo W, Yong CK, Yu JX (2011) Utilization of unmodified gold nanoparticles in colorimetric detection. Science China: Physics, Mechanics and Astronomy. Science in China Press; 2011. pp. 1757–1765. https://doi.org/10.1007/s11433-011-4486-7

35. Yao X, Ma X, Ding C, Jia L (2016) Colorimetric determination of lysozyme based on the aggregation of gold nanoparticles controlled by a cationic polymer and an aptamer. Microchim. Acta. 183: 2353–2359. https://doi.org/10.1007/s00604-016-1876-6

36. Haralick RM, Dinstein I, Shanmugam K (1973) Textural features for image classification. IEEE Trans. Syst. Man. Cybern. SMC-3: 610–621. https://doi.org/10.1109/TSMC.1973.4309314

37. Texture Analysis Using the Gray-Level Co-Occurrence Matrix (GLCM)—MATLAB & Simulink. [cited 26 January 2021]. Available: https://www.mathworks.com/help/images/texture-analysis-using-the-gray-level-co-occurrence-matrix-glcm.html

38. Kwak G-H, Park N-W (2019) Impact of texture information on crop classification with machine learning and UAV images. Appl. Sci. 9: 643. https://doi.org/10.3390/app9040643

39. Tan J, Gao Y, Cao W, Pomeroy M, Zhang S, Huo Y, et al. (2019) GLCM-CNN: Gray level co-occurrence matrix based CNN model for polyp diagnosis. IEEE EMBS International Conference on Biomedical and Health Informatics, BHI 2019—Proceedings. Institute of Electrical and Electronics Engineers Inc. https://doi.org/10.1109/BHI.2019.8834585

40. Vidyarthi A, Mittal N (2017) Texture based feature extraction method for classification of brain tumor MRI. Journal of Intelligent and Fuzzy Systems. 32: 2807–2818. https://doi.org/10.3233/JIFS-169223

41. Abdel-Nasser M, Melendez J, Moreno A, Omer OA, Puig D (2017) Breast tumor classification in ultrasound images using texture analysis and super-resolution methods. Eng. Appl. Artif. Intell. 59: 84–92. https://doi.org/10.1016/j.engappai.2016.12.019

42. Kirby R, Cho EJ, Gehrke B, Bayer T, Park YS, Neikirk DP, et al. (2004) Aptamer-based sensor arrays for the detection and quantitation of proteins. Anal. Chem. 76: 4066–4075. https://doi.org/10.1021/ac049858n PMID: 15253644

43. Chen H, Muros-Cobos JL, Amirfazli A (2018) Contact angle measurement with a smartphone. Rev. Sci. Instrum. 89: 035117. https://doi.org/10.1063/1.5022370 PMID: 29604727

44. Ferguson TP, Qu J (2004) Moisture and temperature effects on the reliability of interfacial adhesion of a polymer/metal interface. Proceedings—Electronic Components and Technology Conference. 1752–1758. https://doi.org/10.1109/ectc.2004.1320355

45. Texture Analyzer. [cited 26 January 2021]. Available: https://imagej.nih.gov/ij/plugins/texture.html

46. Lykhovyd PV (2018) Prediction of sweet corn yield depending on cultivation technology parameters by using linear regression and artificial neural network methods. Biosyst. Divers. 26: 11–15.

47. Sanjay M, Kalpana B (2017) Early mass diagnosis of *Fusarium* wilt in banana cultivations using an E-Nose integrated autonomous rover system. Int. J. Appl. Sci. Biotechnol. 5: 261–266. https://doi.org/10.3126/ijasbt.v5i2.17621

48. Jeddi I, Saiz L (2017) Three-dimensional modeling of single stranded DNA hairpins for aptamer-based biosensors. Sci. Rep. 7: 1–13. https://doi.org/10.1038/s41598-016-0028-x PMID: 28127051

49. Alshaer W, Ababneh N, Hatmal M, Izmirli H, Choukeife M, Shraim A, et al. (2017) Selection and targeting of EpCAM protein by ssDNA aptamer. PLoS One 12: e0189558. https://doi.org/10.1371/journal.pone.0189558 PMID: 29245156

50. Hofacker IL, Lorenz R (2014) Predicting RNA structure: Advances and limitations. Methods Mol. Biol. 1086: 1–19. https://doi.org/10.1007/978-1-62703-667-2_1 PMID: 24136595

51. Biesiada M, Purzycka KJ, Szachniuk M, Blazewicz J, Adamiak RW (2016) Automated RNA 3D Structure Prediction with RNA Composer. In: Turner D, Mathews D (eds) RNA Structure Determination. Methods in Molecular Biology. 1490: 199–215. Humana Press, NY. https://doi.org/10.1007/978-1-4939-6433-8_13

52. Phillips JC, Braun R, Wang W, Gumbart J, Tajkhorshid E, Villa E, et al. (2005) Scalable molecular dynamics with NAMD. J. Comput. Chem. 26: 1781–1802. https://doi.org/10.1002/jcc.20289 PMID: 16222654

53. Brooks BR, Brooks CL, Mackerell AD, Nilsson L, Petrella RJ, Roux B, et al. (2009) CHARMM: The biomolecular simulation program. J. Comput. Chem. 30: 1545–1614. https://doi.org/10.1002/jcc.21287 PMID: 19444816

54. Yan Y, Zhang D, Zhou P, Li B, Huang SY (2017) HDOCK: A web server for protein-protein and protein-DNA/RNA docking based on a hybrid strategy. Nucleic Acids Res. 45: W365–W373. https://doi.org/10.1093/nar/gkx407 PMID: 28521030

55. Xu X, Chen S-J (2016) VfoldCPX Server: Predicting RNA-RNA complex structure and stability. Huang X, editor. PLoS One. 11: e0163454. https://doi.org/10.1371/journal.pone.0163454 PMID: 27657918

56. DeLano W, Bromberg S (2004) PyMOL User's Guide. DeLano Scientific LLC. Available: https://dasher.wustl.edu/chem430/software/pymol/user-guide.pdf

57. Huang FWD, Qin J, Reidys CM, Stadler PF (2010) Target prediction and a statistical sampling algorithm for RNA-RNA interaction. Bioinformatics 26: 175–181. https://doi.org/10.1093/bioinformatics/btp635 PMID: 19910305

58. Bernhart SH, Tafer H, Mückstein U, Flamm C, Stadler PF, Hofacker IL (2006) Partition function and base pairing probabilities of RNA heterodimers. Algorithms Mol. Biol. 1: 1–10. https://doi.org/10.1186/1748-7188-1-1 PMID: 16722576

59. Andronescu M, Zhang ZC, Condon A (2005) Secondary structure prediction of interacting RNA molecules. J. Mol. Biol. 345: 987–1001. https://doi.org/10.1016/j.jmb.2004.10.082 PMID: 15644199

60. Dirks RM, Bois JS, Schaeffer JM, Winfree E, Pierce NA (2007) Thermodynamic analysis of interacting nucleic acid strands. SIAM Rev. 49: 65–88. https://doi.org/10.1137/060651100

61. Zhao C, Xu X, Chen SJ. Predicting RNA Structure with Vfold (2017) Methods Mol. Biol. 1654: 3–15. https://doi.org/10.1007/978-1-4939-7231-9_1 PMID: 28986779

62. Sukhwal A, Sowdhamini R (2015) PPCheck: A webserver for the quantitative analysis of protein-protein interfaces and prediction of residue hotspots. Bioinform. Biol. Insights 9: BBI.S25928. https://doi.org/10.4137/BBI.S25928 PMID: 26448684

63. Shamir L, Wolkow CA, Goldberg IG (2009) Quantitative measurement of aging using image texture entropy. Bioinformatics 25: 3060–3063. https://doi.org/10.1093/bioinformatics/btp571 PMID: 19808878

64. Pantic I, Pantic S, Paunovic J, Perovic M (2013) Nuclear entropy, angular second moment, variance and texture correlation of thymus cortical and medullary lymphocytes: Grey level co-occurrence matrix analysis. An. Acad. Bras. Cienc. 85: 1063–1072. https://doi.org/10.1590/S0001-37652013005000045 PMID: 23969846

65. Sharma N, Ray A, Sharma S, Shukla K, Pradhan S, Aggarwal L (2008) Segmentation and classification of medical images using texture-primitive features: Application of BAM-type artificial neural network. J. Med. Phys. 33: 119–126. https://doi.org/10.4103/0971-6203.42763 PMID: 19893702

66. Ajiboye AR, Abdullah-Arshah R, Qin H, Isah-Kebbe H (2015) Evaluating the effect of dataset size on predictive model using supervised learning technique. Int. J. Comput. Syst. Softw. Eng. 1: 75–84. https://doi.org/10.15282/ijsecs.1.2015.6.0006

67. Pons C, Grosdidier S, Solernou A, Pérez-Cano L, Fernández-Recio J (2010) Present and future challenges and limitations in protein-protein clocking. Proteins Struct. Funct. Bioinforma. 78: 95–108. https://doi.org/10.1002/prot.22564 PMID: 19731373

68. Ramírez D, Caballero J (2016) Is it reliable to use common molecular docking methods for comparing the binding affinities of enantiomer pairs for their protein target? Int. J. Mol. Sci. 17: 525. https://doi.org/10.3390/ijms17040525 PMID: 27104528